ELSEVIER

Journal of Biomechanics 39 (2006) 551–563

JOURNAL OF BIOMECHANICS

www.elsevier.com/locate/jbiomech
www.JBiomech.com

Numerical investigation of non-Newtonian microcirculatory blood flow in hepatic lobule

H.P. Rani[a], Tony W.H. Sheu[a,*], T.M. Chang[b], P.C. Liang[c]

[a]*Department of Engineering Science and Ocean Engineering, National Taiwan University, 73 Chou-Shan Road, Taipei, Taiwan, Republic of China*
[b]*National Defense Medical Centre, Taipei, Taiwan, Republic of China*
[c]*National Taiwan University Hospital, Taipei, Taiwan, Republic of China*

Accepted 24 November 2004

Abstract

The circulation in the liver is unique at macroscopic and microscopic levels. At the macroscopic level, there is an unusual presence of portal and arterial inputs rather than a single arterial input. At the microscopic level, a series of microenvironments in the acinar system is essential in controlling the functional characteristics of hepatic parenchymal cells. Since the hemodynamics is much less studied in the multifunctional liver, an attempt is made to study the hepatic hemodynamics in a segment of a hepatic lobular structure, that is made up of high-pressure oxygenated arteriole, low-pressure nutrient-rich portal venule, fenestrated sinusoidal space and hepatic venule. Our goal is to dispel some of the myths of this complex vascular bed by means of finite volume blood flow simulation. Flow features like high-velocity gradients near the fenestrations, flow reversal and Dean vortices in the sinusoidal space are analyzed within the non-Newtonian framework. Since no distinct exact or numerical solutions are available for this complex vascular bed, the present simulated results are compared with the available clinical observations. Results revealed that the pressure plays a key role in hepatic blood flow.

Keywords: Microcirculation; Acinus; Hepatic lobule; Non-Newtonian blood flow

1. Introduction

The intimate relationship between liver blood circulation and diseases, such as fibrosis, cirrhosis, portal hypertension and heptocellular carcinoma, has been known for years (Lautt, 1980). In addition, the importance of microcirculation can be felt during ischemia and reperfusion. When microcirculation deteriorates, liver tissues fail to receive proper nutrition and oxygen and can cause fibrosis (scar formation) and other complications to occur. Previous studies (Villeneuve et al., 1996; Seeff, 2002) revealed that the chronic viral hepatitis patients suffer, in particular, with the microcirculation disorders (or blood stagnancy in Chinese medicine). By improving microcirculation in the liver, the liver cell can regenerate and suppress hypertrophy of the interstitial connective tissue, thus preventing many liver diseases. In the case of liver failure, one promising alternative is to replace the diseased liver with an extracorporeal bio-artificial liver (BAL). In essence, the BAL is a bioreactor containing cultured hepatocytes that function as the extracorporeal liver on a temporary basis (Ledezma et al., 1999; Sllen and Bhatia, 2002) as liver cells have the capacity to regenerate themselves (Michalopoulos and DeFrances, 1997). Hence a thorough understanding of liver microcirculation is important for refining designs of the BAL and for the surgical planning tools (Selle et al., 2002).

A detailed exploration of hepatic microcirculation has been focused on the two primary models known as the lobular model and acinar model (Lebouton, 2000; Andrews, 1979; Arias et al., 1988). In the hepatic

*Corresponding author. Fax: +886 2 23929885.
E-mail addresses: ranihkg@yahoo.com (H.P. Rani), twhsheu@ntu.edu.tw (T.W.H. Sheu).

0021-9290/$ - see front matter © 2005 Elsevier Ltd. All rights reserved.
doi:10.1016/j.jbiomech.2004.11.029

lobular model, the liver has been paralyzed into lobules. Lautt (1980) pointed out that this microscopic lobular model could explain the flow distributions like blood flow and blood volume. The circulating blood reaches the hexagonal lobule via portal tracts and drains via central venules, which are tributaries of the hepatic vein. This basic hexagonal pattern is replicated millions of times throughout the tissue. Each portal tract contains branches of the hepatic artery, lymph ducts and bile ducts in addition to a distributor branch of the hepatic portal vein. This model schematic in Fig. 1 is represented for calculating the amount of blood in the hepatic microciculatory system. The amount of blood in the investigated hepatic microcirculatory system depends on the system's pressure. Katz and Rodbard (1939) found that the pressure variation played a key role in the hepatic microcirculation and in cardiac functions. Also, the variation in pressure is an important factor to determine the volume of the blood that is contained in the liver. Mountcastle (1968) regarded the hepatic vessel as the vehicle for offering a more or less constant resistance. When the mesenteric vessels constrict, the portal system would be relatively empty and the extra blood would be available for use elsewhere.

Paton et al. (1992) gave a detailed account of the acinar model. They explained that this model's morphological boundaries can change with metabolic differences in the liver. In this hepatic acinar model, the portal tract is at the centre and a line surrounding the terminal hepatic venule (HV) defines the outer boundary. Within the acinus, there are three metabolic zones namely zone I, zone II and zone III. Zone I is closest to the portal tract, zone III lies near the HV whereas zone II is in between zones I and III. For clarity, the model under current investigation is schematically represented in Fig. 2. This acinar arrangement of the vascular system creates a series of microenvironments, which are acknowledged with importance in controlling the functional characteristics of the parenchymal cells.

The pioneers Rapport and McCuskey have reported the detailed experimental study for the assessment of both local blood supply and liver function. Ruijter et al. (2000) and McCuskey (1994) detailed in their studies about the sinusoidal space connection with the portal tract and HV. This anastomose sinusoidal space consists of endothelial cells and fenestrations. According to Arias et al. (1988) this sinusoidal space is made up of approximately 18–20 endothelial fenestrations. Scherphof et al. (2002) explained that in the hepatic microcirculation, the liver's functional cell, namely, the

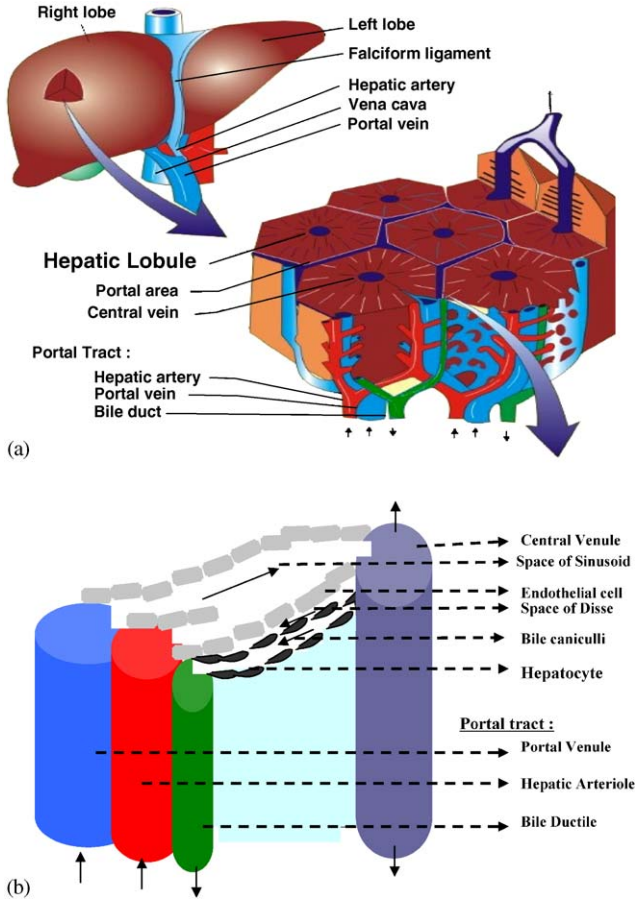

Fig. 1. Schematic of (a) hexagonal hepatic lobule and portal tract (hepatic artery, hepatic vein, bile duct) from liver and (b) segment of hexagonal hepatic lobule consisting of portal tract, liver cells (endothelial cell, hepatocyte), blood flow spaces and central venule (or HV). The arrows indicate the directions of the blood, lymph and bile flows in the space of sinusoid, space of disse and bile caniculli, respectively.

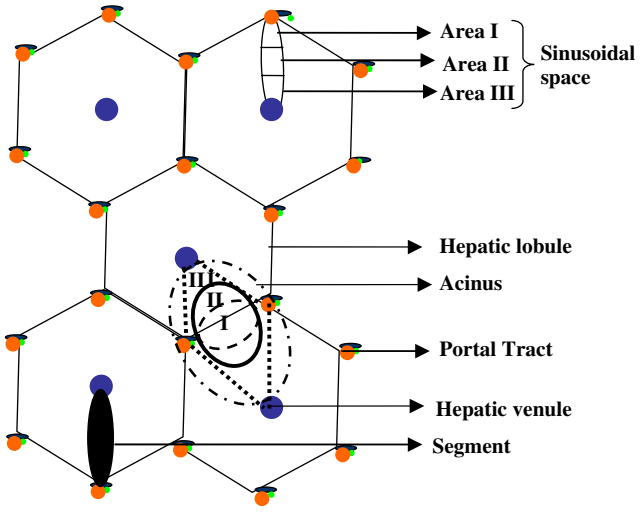

Fig. 2. Schematic of a cross section of hepatic parenchyma, which consists of the sinusoidal space (area I (presinusoidal), area II (interasinsoidal) and area III (post-sinusoidal)), the hexagonal hepatic lobule, acinus with the three zones (zones I, II and III), portal tract (inlet), the HV (outlet) and the investigated segment of a hepatic lobule (shaded area).

hepatocyte must collide with the endothelial wall of the sinusoid before a blood solute can come into contact with it, pass through the endothelial fenestrations and then enter into the space of Disse (Fig. 1b). Within the space of Disse, the microvilli of the hepatocyte provide an amplified surface area for uptake of oxygen and nutrients. The probability of the eventual collision between solute and hepatocyte membrane is therefore a function of hemodynamic and structural parameters. Typical of these parameters are the velocity and pressure of the blood flow, the sinuosity or the degree of branching of the sinusoidal channels, the cross-sectional area and the surface to volume ratio of the sinusoidal space, the total area of endothelial fenestrate, and the surface area of available hepatocyte membrane. The existence of significant morphological differences in one or several of these factors within the three zones of the hepatic acinus could conceivably cause solute–membrane interactions to occur in each acinar zone. This concept is important in determining the contribution of hepatocytes in each acinar zone pertaining to solute uptake and in predicting the solute concentration gradients across the acinus.

Usually biomechanics studies focus on the microcirculatory phenomena related to function on the cellular level in general and on phenomena occurring at the microvascular wall in particular. The liver is unique because of the two inlet flows and the presence of capillary segments in the terminal vascular bed. In the liver, the interface between blood and tissue is the sinusoidal lining surface in lieu of the normal microvascular endothelium. Hence, the interaction between the blood cells and the vascular wall tends to take place at the surface of the sinusoidal lining cells. In the event of this interaction, either altered or impaired, the blood cells would directly interact with hepatocytes and/or Kupffer cells. Since much less attention has been paid to this complex vascular bed so far, an attempt is made to understand some of the three-dimensional non-Newtonian blood flow characteristics in the hepatic lobular model using computational fluid dynamic techniques. One of the most important and challenging problems in the hepatic vasculature is to reveal how the low-pressured portal blood can flow into the sinusoids that are filled with arterial blood of eight times higher pressure. The results discussed in the present study will hopefully gain currency especially for liver surgery and liver transplantation.

A segment of a hexagonal hepatic lobule as shown in Figs. 1 and 2 was considered for the present study. The lobule represents a small parenchymal mass that consists of the terminal hepatic arteriole (HA), terminal portal venule (PV), sinusoidal space with fenestrated endothelial cells and terminal HV. A reputed software (CFDRC, CFD Research Corp., Huntsville, AL) was used to study the current problem. The proposed three-dimensional hepatic lobular model was constructed and the blood flow was initiated using the available parameters. The hepatic blood in this model was considered as non-Newtonian. The blood properties in the HA and the PV were assumed to be of different types. The constitutive equations, like the Power law model and the Walburn and Schneck model for non-Newtonian fluid, were used to study this problem at length. The blood viscosity changes with respect to vessel diameter were studied for the shear thinning blood. The hepatic flow characteristics are analysed by means of velocity, pressure and mass flow rate in the HA, PV, sinusoidal space and HV. The simulated results are thus compared and validated with the concepts and findings of distinguished scientists and clinicians in the field of hepatology.

In Section 2, the proposed hepatic lobular model is explained in detail. The governing equations and numerical method for the present hepatic model are given in Section 3. Section 4 deals with the simulated complex flow structure with the help of a well-developed software. In addition to validation of the results, the insight of physical parameters like velocity, pressure and strain rate are included. The conclusions are drawn in the last section.

2. Problem description

In the present paper, PV and HA with extended bifurcation branches that drain the circulating blood into the fenestrated sinusoidal space and open-ended HV were considered for the model schematic as shown in Fig. 3. In each sinusoidal space, 18 fenestrations were considered. The sinusoidal space which is close to the HA and PV was considered as presinusoidal and mentioned as area I. The sinusoidal space which is located near the HV was considered as post-sinusoidal (area III). The intermediate sinusoidal space between areas I and III was considered as interasinusoidal space (area II). The three areas are part of the three zones in the acinar model and are depicted in Fig. 2. This hepatic lobular model employs most of the dimensions described by Lautt (1980). The dimensions used in the present model are tabulated in Table 1.

The PV blood and HA blood are assumed to have different properties. The arterial blood properties like density (ρ) and viscosity (η) are taken to be $1050\,kg/m^3$ and $0.035\,g/(cm\,s)$, respectively (Bovendeerd et al., 1987). The PV blood is known to be more viscous and denser than the arterial blood, as it contains nutrient-rich blood of the intestine and spleen (Lebouton, 2000; Andrews, 1979; Arias et al., 1988; Lautt, 1980). Therefore, it is assumed that the density and viscosity of the PV blood are $2000\,kg/m^3$ and $0.35\,g/(cm\,s)$, respectively (Gleen, 1998–2004, Svihus et al., 2000). The vessels are assumed to be rigid and the velocity conditions are of

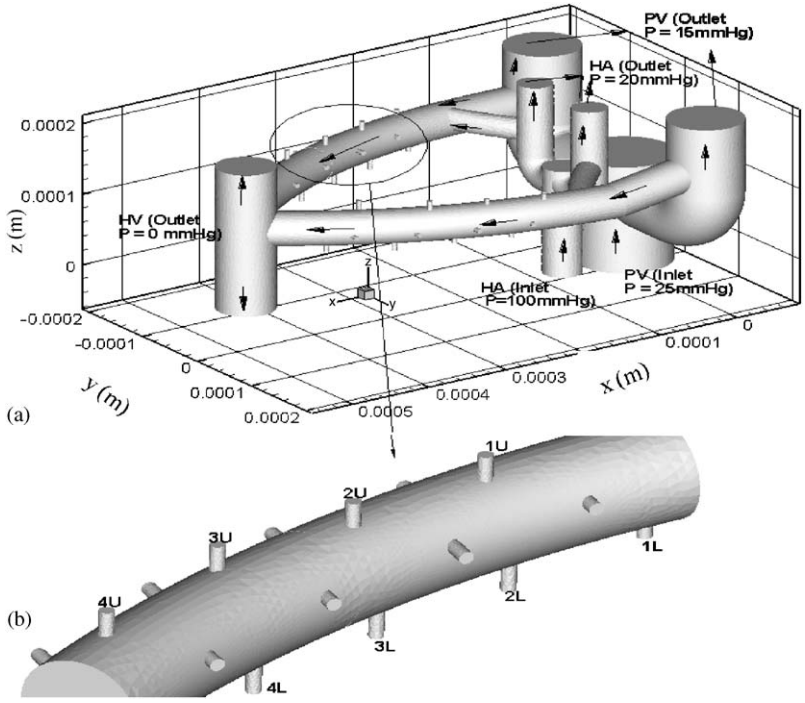

Fig. 3. (a) The investigated three-dimensional hepatic lobular model, which consists of inlets (hepatic arteriole (HA), portal venule (PV)), outlets (fenestrations and hepatic venule (HV)) and (b) enlarged sinusoidal path with the markings of lower (1L, 2L, 3L, 4L) and upper (1U, 2U, 3U, 4U) fenestrations.

Table 1
Dimensions used in the simulation of hepatic lobular model

Model dimensions (μm)	HA	PV	Fenestrate	HV	Sinusoidal space	Endothelial cell
Radius	22	53	2.5	33	23.5	—
Height	250	250	4–5	250	—	—
Length	—	—	—	—	250	10

no-slip and no-penetration types on the wall. The blood motion is assumed to be solely driven by pressure. A fixed pressure boundary is used to keep a constant pressure drop from the inlet to outlet. The boundary conditions for the current model include the fully developed inlet flow. At the exit, the flow is assumed to have zero gradient and zero normal velocity. The inlet/outlet (P_{in}/P_{out}) pressure values (Bezy-Wendling et al., 2003) of the microvessels are listed in Table 2. The outlet pressure values of each vessel were prescribed as initial conditions to initiate the flow. Initially, except the PV all other microvessel's viscosity and density values are assumed to have the same values of the HA.

In microcirculation, the Reynolds number (*Re*), with respect to the individual red blood cell, is very small to make a creeping flow assumption (Fung et al., 1972; Fung, 1993; Chang et al., 2000) valid. Hence in the present study, *Re* is assumed to have a value less than one.

Table 2
The pressure values used in the simulation of hepatic lobular model

Pressure (mm Hg)	HA	PV	Fenestrate	HV
P_{in}	95	25	—	—
P_{out}	20	15	2	0

3. Governing equations and numerical methods

In the present microcirculatory hepatic lobular model, the red blood cells (approximately 7 μm in diameter) undergo very large extension and severe deformation (Fung et al., 1972; Chang et al., 2000, Branemark and Lindstrom, 1963) especially in the fenestrations (5 μm in diameter). Also, the shear thinning and viscoelasticity of blood (Chien et al., 1970; Thurston, 1973, 1979; Fung, 1996) are closely related to its microscopic structures,

e.g., aggregation, deformation and alignment of the red blood cells. This implies that the red blood cells determine mainly the rheological behavior of the blood. Hence, it is customary to consider the non-Newtonian assumption in the following unsteady three-dimensional incompressible Navier–Stokes equations:

$$\rho\left(\frac{\partial \bar{V}}{\partial t}+(\bar{V}\cdot\nabla)\bar{V}\right)=-\nabla P+\nabla\bar{T}. \quad (1)$$

In the above, $\bar{V}$, P and t represent the dimensionless velocity vector ((u, v, w) in (x, y, z) directions), pressure and time, respectively. The stress tensor $\bar{T}(\equiv 2\eta(\dot{\gamma})\mathbf{D})$ linearly depends on the rate of deformation tensor $\mathbf{D}\left(=\frac{1}{2}(\nabla\bar{V}+\nabla\bar{V}^T)\right)$. For a non-Newtonian fluid, the density (η) is a function of shear rate ($\dot{\gamma}$) while for a Newtonian fluid η has a constant value and is independent of the shear rate. The divergence-free condition is imposed on the velocity by

$$\nabla\cdot\bar{V}=0. \quad (2)$$

The proposed hepatic microcirculatory system was analyzed by commercially available finite volume software, namely, the CFDRC (CFD Research Corp., Huntsville, AL) for gaining the physiological insight. The central programs of this software are the CFD-GEOM for geometry and grid generations, the CFD-ACE for flow solver and the CFD-VIEW for post-processing. A convenient graphical user interface (GUI) is provided for specifying the required fluid properties, boundary and initial conditions. By using the same GUI, solver options for assigning relaxation parameters, a number of iterations and interpolation schemes were also set.

In the first analysis phase, the geometry of the flow model has been constructed with reference to the hepatic lobule. This model is schematically shown in Fig. 3. In the mesh generation, triangular and tetrahedral meshes were created. About 450934 mesh points were used in this tetrahedral mesh. The upwind spatial differencing for approximating convective terms and the CGS pre-conditioning technique for accelerating convergence were the chosen options to solve the velocity and pressure solutions in Eqs. (1) and (2). In the current transient simulation, the first-order time accurate Euler's method was used. The convergence criterion set for the present study was 1E-15. During a simulation, files containing flow properties were produced. The results were analysed in detail with an aid of plotting and animation embedded in the post-processor.

4. Results and discussion

4.1. Validation

As there are no exact or numerical solutions available for this hepatic lobule structure, the validation was done with a 180° sharp bend benchmark problem. This 180° bend problem, schematic in Fig. 4a, is featured with the curvature ratio $R/D=13$, where R is the radius of curvature and D is the hydraulic diameter. The inner width and height of the duct were taken as 1.0. The length of the duct before and after the bend was taken as 10 times of the hydraulic diameter. At the inlet, a fully developed velocity profile was specified. Simulation was performed at $Re=574$. The simulated radial variations of azimuthal velocity shown in Fig. 4b are compared well with those in Chung et al. (2003) at $\Phi=18°$ along the mid-span of the duct.

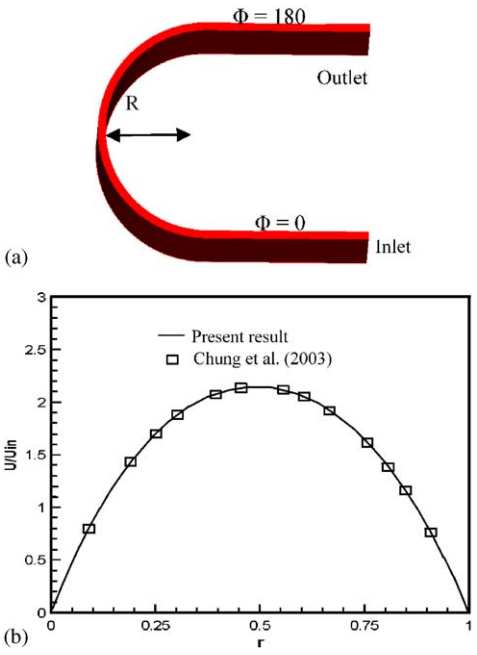

Fig. 4. (a) Schematic of the U-bend flow problem for validation purpose and (b) a comparison of the simulated and experimentally measured main stream velocities at different radial locations.

4.2. Convergence and gird independency

The residual values of the velocity and pressure against the iteration number were calculated. It was observed that the convergence criterion 1E-15, set in the GUI was reached at 171st iteration. Subsequent decrement and increment in mesh resolution by 50% were applied to evaluate if the employed mesh resolution was adequate to obtain accurate solutions. It was observed that when the mesh resolution was decreased by 50%, the axial velocity profile also decreased and maximum relative error was 13% of the currently employed mesh velocity profile. As the present mesh resolution was increased by 50%, the axial velocity profile did not change more than 1%. These results suggest that the current mesh resolution is sufficient to obtain grid-independent solutions for the proposed model.

4.3. Investigating blood models

To investigate the efficiency of blood models, the fluid properties of the model were assumed to be same everywhere. The blood properties like density and viscosity were taken to be 1050 kg/m^3 and 0.035 g/(cm s), respectively. The shear thinning effect was taken into account by applying the Power law model and the Walburn and Schneck model (1973) to determine viscosity. The Power law model is represented as $\mu = \lambda|\dot{\gamma}|^{n-1}$, where $\lambda(\mu) = \mu_\infty + \Delta\mu \exp\{-(1 + (-|\dot{\gamma}|/a))\} \exp(-b/|\dot{\gamma}|)$ and $n(\mu) = n_\infty + \Delta n \exp\{-(1 + |\dot{\gamma}|/c)\} \exp(db/|\dot{\gamma}|)$. The default settings used in CFD-ACE are tabulated in Table 3. The Walburn and Schneck model is given by

$$\mu = a_1 \exp[(a_2 H + a_3/H^2)\dot{\gamma}^{(1-a_4 H)}],$$

where H denotes the blood Hematocrit. The default settings are given in Table 3.

In general, studies on shear thinning blood rheology are restricted to regions at relatively low shear rates (Hron et al., 2000). This means that there should be a transition of constitutive equations switching from non-Newtonian fluid to Newtonian fluid. Fig. 5a shows the non-Newtonian viscosity for the two constitutive equations and for the Newtonian flow. It is observed that in the Power law model, blood viscosity is constant at higher strain rates. Hence, the Power law equation recovers the Newtonian model under the high strain rate circumstances. In the Walburn and Schneck model, we can specify the hematocrit. The disadvantage of this model is that the viscosity keeps decreasing as a function of strain rate (Bitsch, 2002). It is observed that the viscosity in the blood vessel is higher in the core and lower at the wall (Fung, 1993; Das et al., 1998). This viscosity difference can affect the velocity profile.

Table 4 explains the relationship between the hepatic microvessel diameter and the blood viscosity. The observed proportional relationship indicated that the viscosity was decreasing with the decreasing vessel diameter. The blood viscosity is, however, found higher in the PV than in the fenestrations. A similar trend was also reported by Fahraeus and Lindqvist (1931), who tested blood flow in glass tubes connected to a feed reservoir of diameter in the range of 500–50 μm.

The axial velocity profiles for the Newtonian and non-Newtonian (Power law model) fluids are shown in Fig. 5b. The centerline axial velocity variations are calculated at the cross section of the sinusoidal space. The results indicated that the axial velocity in the present hepatic lobule for a Newtonian fluid is parabolic but for the non-Newtonian fluid it is normally flattened. This flattened velocity profile is due to the blood shear thinning property.

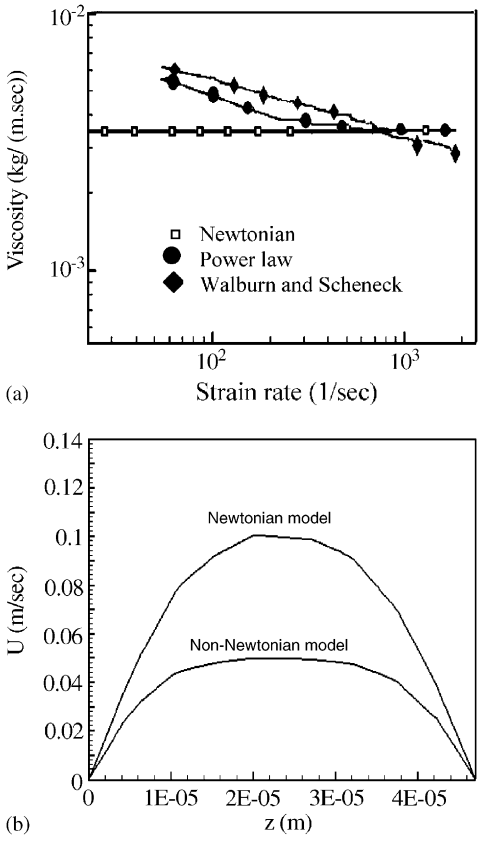

Fig. 5. (a) The simulated non-Newtonian blood viscosities for two investigated blood models and Newtonian blood viscosity against the strain rate and (b) the simulated axial velocity profiles in area I for the Newtonian and non-Newtonian blood flows.

Table 3
Parameters used in the Power law model and Walburn and Schneck model

Power law parameter	Value in CGS units	Walburn and Schneck parameter	Value in CGS units
μ_∞	0.035	a_1	0.00797
$\Delta\mu$	0.25	a_2	0.0608
N_∞	1.0	a_3	377.7515
Δn	0.45	a_4	0.00499
a	50.0	—	—
b	3.0	—	—
c	50.0	—	—
d	4.0	—	—

Table 4
The change of blood viscosity with the size of blood vessel

Vessel (diameter in μm)	Viscosity (kg/(m sec))
Portal venule (106)	7.3E-3
Sinusoidal space (47)	4.3E-3
Hepatic arteriole (44)	3.5E-3
Fenestration (5)	3.3E-3

4.4. Flow features

In this section, the main features of the investigated hepatic lobule like the higher velocity gradients near the fenestrations, the flow reversal and Dean vortices in the sinusoidal space are explained and discussed in detail. In the HA and PV, both density and viscosity of the blood were assumed to be of different types. The density and viscosity of blood in the HA and the PV are already mentioned in the problem description section. The upcoming three-dimensional, non-Newtonian hepatic flow results will be calculated using the Power law model.

Different pressure values were simulated in different vessels in order to study the blood flow in the hepatic lobule, as shown in Fig. 6. A high pressure was simulated at the HA than those in the other vessels. This highest pressure in the HA initiated the blood flow in the hepatic lobule. It is observed that the blood flow is continuous even after the pressure drop occurred at the HA. This tendency is due to different pressure gradients that existed across the PV, sinusoidal space and the HV. Since area I is located near the HA and PV, more amount of blood flow is observed than those in areas II and III.

The pressure values across different vessels in hepatic lobule were calculated when there was a peak pressure in the HA. It was observed that a high pressure was occurred at the sinusoidal entrance (HA + PV) in the sinusoidal space due to its proximity to the HA and PV. At a time when there was a peak pressure in the HA, the axial velocity across the hepatic vessels was found decreased from area I to area III. A reduced velocity was also seen in the HV.

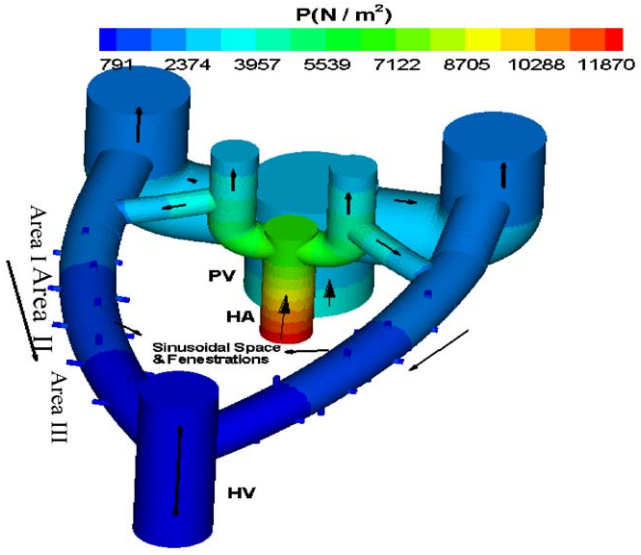

Fig. 6. Initially simulated pressure contours for the investigated hepatic lobule.

The simulated pressure variations against time in the HA + PV, areas I, II and III are shown in Fig. 7. Initially the pressure suddenly increased with time and reached a peak value at 5E-6 s. Then they gradually decreased with time and reached a steady state. It is also observed that the simulated pressures decreased from area I to area III.

The simulated velocity variations with respect to time in the HA + PV, areas I, II and III are shown in Fig. 8. It is observed that velocity increased with time and reached a steady state after time $t = 5E-5$. Also, the velocity decreased from the sinusoidal entrance (HA + PV) to area III. Higher velocities are observed in the sinusoidal entrance in comparison with those in areas I, II and III. The reason may be attributed to the fact that the HA + PV is located near the portal tract. Hence, this

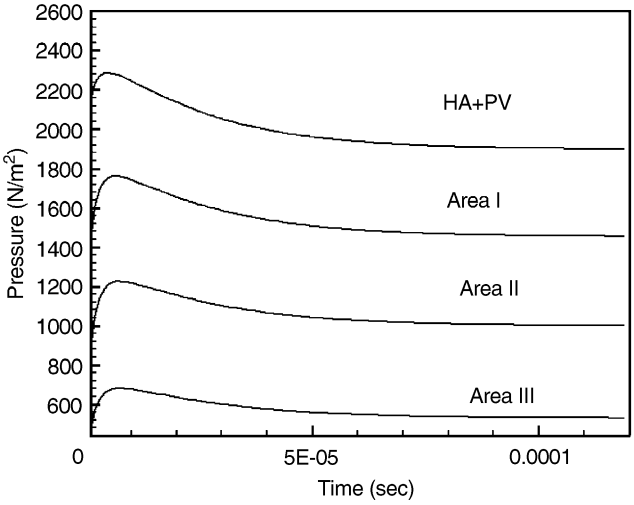

Fig. 7. The simulated pressure variations with respect to time in the sinusoidal space.

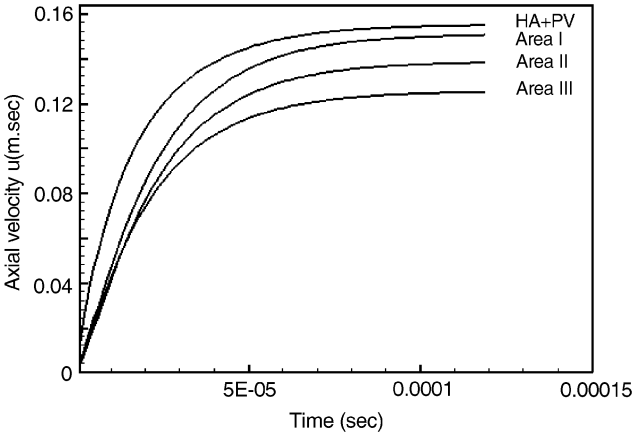

Fig. 8. The simulated axial velocity profiles in the sinusoidal space with respect to time.

entrance region has a tendency to receive blood from the HA or PV all the time.

An attempt is, hence, made to explain how the PV blood at the low pressure condition could flow into sinusoids that received arterial blood of eight times higher pressure based on the simulated results. The flow phenomenon in the hepatic lobule is the consequence of intermittent activity of the HA. According to Lautt (1980) and MacPhee et al. (1993), intermittent activity is normally controlled by nerves or Kupffer cells, thereby rendering opening and closing of the arteriolar sphincters. The arteriolar gate (inlet sphincter) is opened when the high pressure is simulated at the HA. Hence, the pressure at the sinusoidal entrance (HA + PV) rises rapidly as shown in Figs. 6 and 7. High-pressure blood from HA spurts into the sinusoids and sweeps the low-pressure portal blood into the regions ahead of areas I, II, III and HV, without mixing the HA blood and the PV blood. When the pressure drop occurred in the HA, the arteriolar gate (sphincter) closed. However, the portal blood could still flow in the hepatic lobule due to the gradients established in the PV, the sinusoidal space and the HV. This portal blood flow is illustrated in Fig. 8. This phenomenon confirmed the finding of Lautt (1980) that there is no mixing of arteriole and venule bloods in the microcirculatory hepatic lobule.

The simulated pressure contours and streamlines for the hepatic lobule (Fig. 9(i)) along various cross sections are shown in Fig. 9. It is observed that the simulated pressure is maximum at the HA, as compared to those obtained in other vessels. As noticed from Fig. 9(ii), the simulated pressure was found to have a maximum value at area I as compared to areas II and III. It is also observed that the blood at the rear end of the sinusoidal space became dilated due to the low pressure present in the sinusoidal space. Therefore, the pressure contours in Figs. 9(ii, iii) appear light in area III. The streamlines along this z-cross section shown in Fig. 9(iii) explain the flow behavior in three areas I, II and III. It was found that the amount of blood flow in area I was larger than those in the other areas. Also seen are the small eddies present near the intersection planes of the fenestrations and sinusoidal space (Figs. 9(ii, iii)). The eddy formation in the intersection planes of fenestrations and the sinusoidal space is depicted in Fig. 9(iv). Here the eddy forming the secondary flow is due to the geometry effect (Hron et al., 2000). It is observed that the eddy size decreases with an increase in the area level. This phenomenon might be due to the decrease of pressure and velocity with the increase of values computed in areas I, II and III (see Figs. 6–8). The mass flow rate in three areas was calculated, when there was a maximum flow from the HA. The mass flow rates of blood in areas I, II and III were found as 60.98%, 27.35% and 10.9%, respectively. This result reports that cells in area I have the possibility to receive more blood. This occurrence implied that in area I the liver cells have a tendency of receiving larger amounts of blood than those in the other areas. As a result, area I cells are nourished with oxygen from the HA and nutrients from the PV. This may be one of the reasons that the functionality of liver cells, namely, the hepatocytes present in area I differ from those in areas II and III.

The simulated streamlines at the axial cross sections of the PV, HA and HV with a detachment/separation lines in the blood flow are shown in Fig. 9(v). The entry flow in these vessels is detached because of the presence of two bifurcations in the PV/HA. A similar detachment line is also noticed as the flow exits from the HV, where detachment occurred due to the presence of two exits.

Arias et al. (1998) discussed the differences in the functionality of cells present in acinus model at length. They showed that the functional capabilities of the hepatocytes exhibit a gradient along the sinusoidal space. According to them, zone I hepatocytes remove the nutrients and oxygen present in the blood and deplete the supply of nutrients and oxygen to the hepatocytes in zones II and III in the hepatic lobule as the blood flows through the sinusoids. Thus, there are zones of successively less well-oxygenated liver cells within the acini especially in zone III. This phenomenon reveals why many drugs can chiefly damage zone III hepatocytes. Interestingly, a contrast report was also seen for the bile flow (Arias et al., 1988). They argued that zone I hepatocytes tended to suffer greater damage than zones II and III hepatocytes due to the bile flow moving towards the portal tract (Fig. 1) when the bile flow is obstructed. Hence as per the findings of the earlier studies and the obtained results, it is concluded that the drug-induced injuries tend to differentially affect different parts of the sinusoidal space.

According to Daemen et al. (1989), approximately 80% of the macrophages (or Kupffer cells) in the body reside in the sinusoids of the liver. Bouwens et al. (1986) indicated, however, that the percentages of the Kupffer cells were estimated to be 43% in zone I, 28% in zone II and 29% in zone III. According to these findings in the distribution of the Kupffer cells in the three zones and according to the present simulated results of greater blood drainage in area I, there is a need for more macrophage action in area I of the sinusoidal space. Similar results were also reported by MacPhee et al. (1993), who found more Kupffer cells in zone I, as compared to those in zones II and III.

The pressure variations along the sinusoidal cross sections located at different fenestrations were plotted in Fig. 10 under the simulated conditions. In Fig. 10, the markings 1L, 2L, 3L and 4L show the fenestrations that are located in the lower sinusoidal path whereas the 1U, 2U, 3U and 4U represent the fenestrations located in the upper sinusoidal path. The locations are clearly depicted

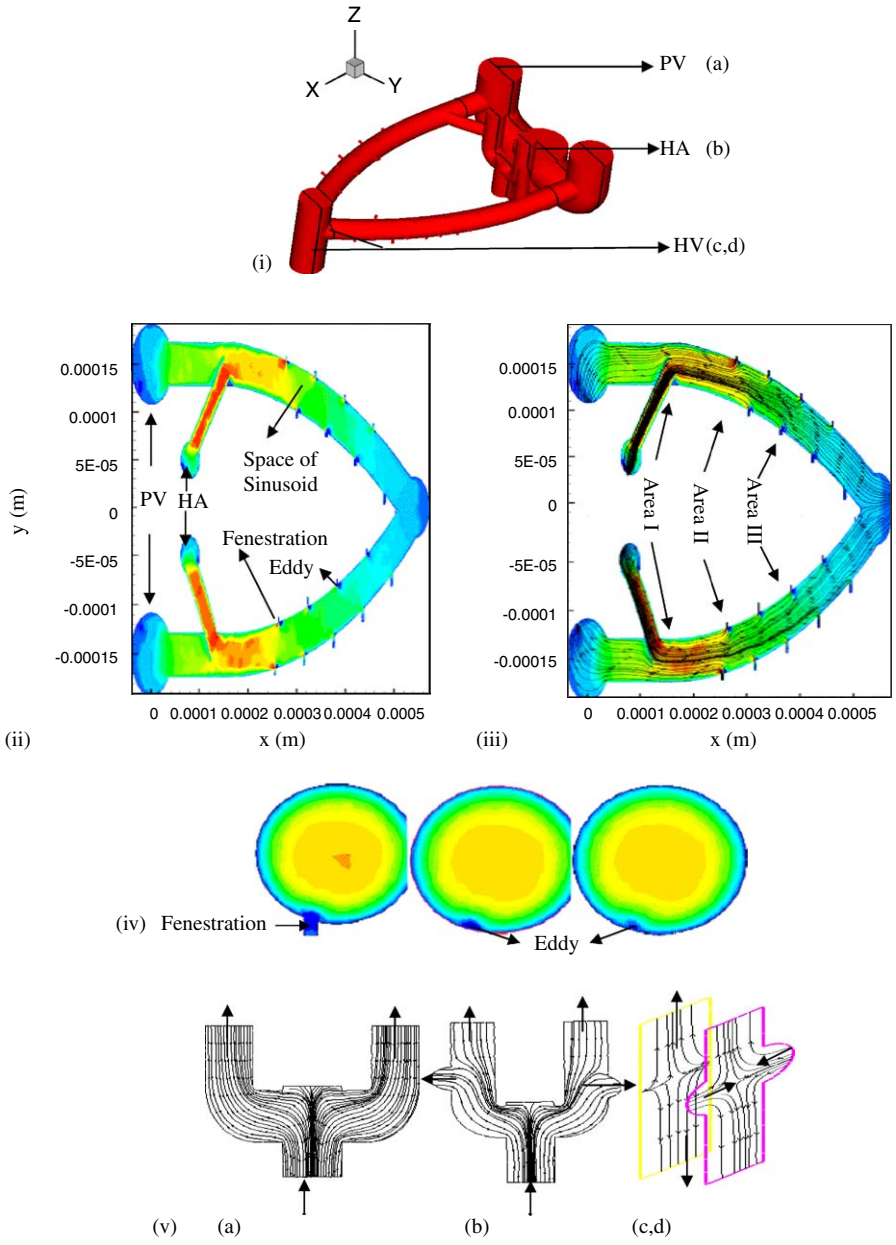

Fig. 9. (i)The investigated hepatic lobular structure showing the locations of axial cross sections, (ii) the simulated pressure contours in z-cutting plane, (iii) the simulated stream lines in z-cutting plane, (iv) the eddy formation at the axial intersection planes of space of sinusoid and fenststration. (colour gradation is shown in Fig. 6), (v) simulated streamlines for the locations shown in (i) (The arrows indicate the directions of the hepatic blood flow).

in Fig. 3. It is found that the pressure in the first (1L, 1U) fenestrations is higher than that of the lower (4L, 4U) fenestrations. Since 1L and 1U fenestrations are located near the simulated high-pressure portal tract, they are subjected to higher pressure than those of 4L and 4U located away from the portal tract.

In Fig. 11, the simulated axial pressure contours at area III fenestration, 4U (shown in Fig. 3) are shown at two different time levels. The pressure contours in Fig. 11a imply that area III fenestration at initial time has no flow reversal. The pressure contours in Fig. 11b were obtained when there was a pressure drop in the HA. It was observed that the pressure drop occurred in the HA while the flow reversed its direction and turned towards the afferent microvessels. Hence a sufficiently high HA pressure was required to make the blood flow unidirectional in the sinusoidal space. Such a similar observation was noticed by Watanabe et al. (1994). Again, these pressure distributions replicated the observation of Katz and Rodbard (1939). They explained why the portal pressure decreased when a back flow occurred in zone III or in the post-sinusoidal space.

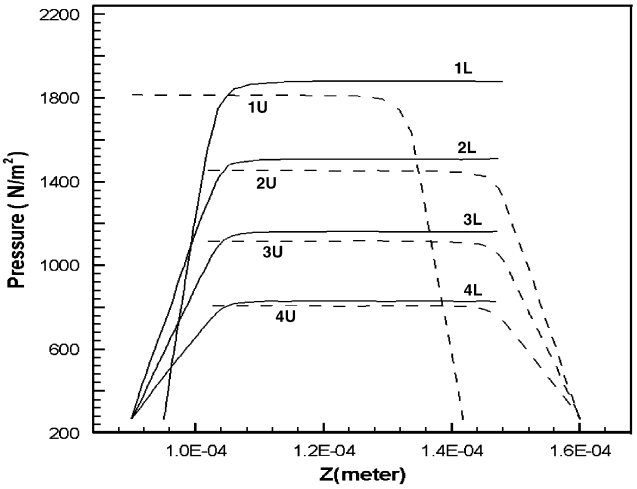

Fig. 10. The simulated axial pressure variations at several cross sections along the lower (1L, 2L, 3L and 4L) and upper (1U, 2U, 3U, 4U) fenestrations. The locations of lower and upper fenestration are shown in Fig. 3.

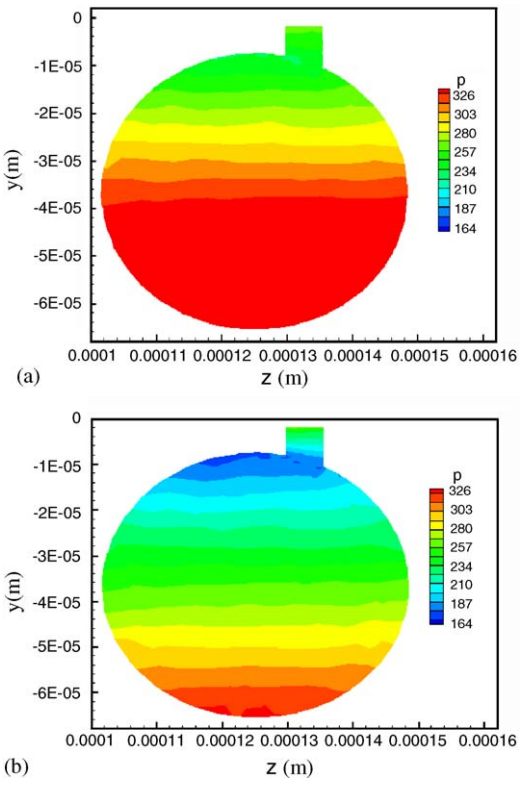

Fig. 11. The simulated pressure contours in area III fenestrate (4U) at different times (a) $t = 5E-6$ and (b) $t = 6E-5$. The location of 4U is shown in Fig. 3.

The centerline sinusoidal velocity profiles of the sinusoidal path at different axial cross sections are plotted in Fig. 12. As expected, the peak velocity is found at the centre of the channel. The velocity decreased as the distance between the portal tract (HA, PV) and the sinusoidal space increased. The

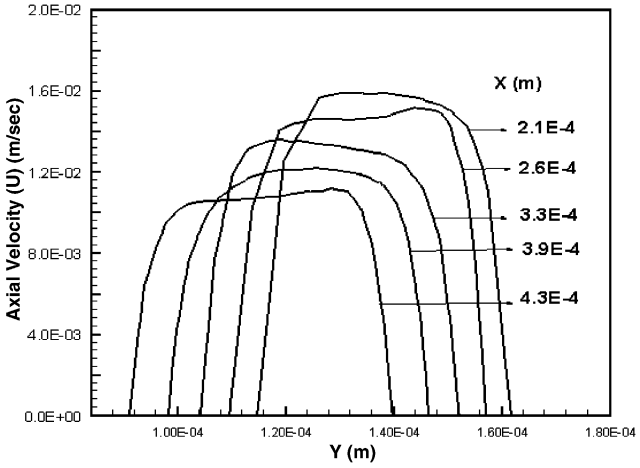

Fig. 12. The simulated velocity profiles at five chosen axial cross sections in the planar sinusoidal space with different fluid properties in the HA and PV.

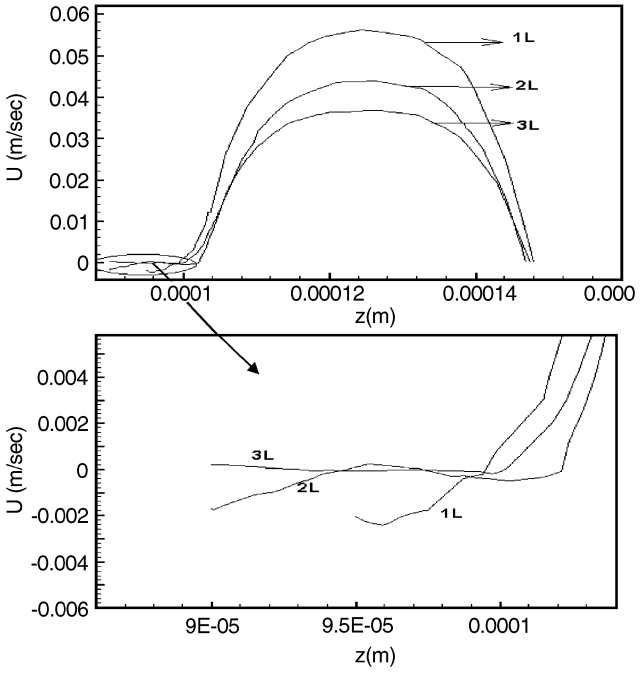

Fig. 13. The simulated axial velocity profiles and their enlarged profiles in the lower (1L, 2L, 3L, 4L) fenestrations. The location of lower fenestrations are shown in Fig. 3.

velocity profiles for the lower (1L, 2L, 3L) fenestrations (Fig. 3) are shown in Fig. 13. The axial velocity distribution gives an indication of the complex flow phenomena in the fenestrated region. When the blood entered the bifurcation (fenestrate), it was split by the apex. As a result, high-velocity gradients are expected near the fenestrate of the divider wall from the sinusoidal space (Fig. 13). The faster moving blood is swept towards the (intersection of sinusoidal space and

fenestrations) divider wall and is replaced by the slower moving blood particles present near the non-divider wall (sinusoidal space). The blood near the divider wall is transported circumferentially towards the non-divider wall. This secondary flow pattern resulted in a Dean vortex as shown in Fig. 14. Hence counter-rotating vortices (Dean vortices) are evident at sections close to the bifurcation. The increase in the cross sectional area gave an adverse pressure gradient too. The blood is, thus, decelerated. The low impetus blood near the non-divider wall is particularly affected by this adverse pressure gradient. The flow reversal near the non-divider wall is seen at every intersection plane of the sinusoidal space and fenestrations. The fenestration curvature induced this pressure gradient. The flow features like the high-velocity gradients near the divider wall of fenestrations, the flow reversal near the non-divider wall of sinusoidal space, and the Dean vortices are predicted by Gijsen et al. (1999) and Chen and Lu (article in press). Another observation made is that the Dean vortices at the rear end of the fenestration decreased with the area level. The reason is that decreasing pressure and velocity go along with the increasing area level, as shown in Figs. 10 and 12.

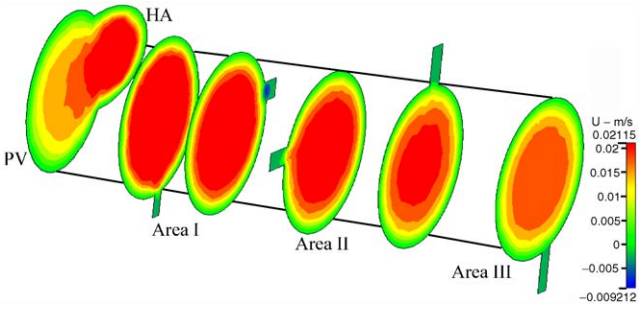

Fig. 14. The simulated axial velocity contours in the hepatic lobule. The velocity contours at axial cross sections from the entry point of sinusoidal space (HA + PV) to area III.

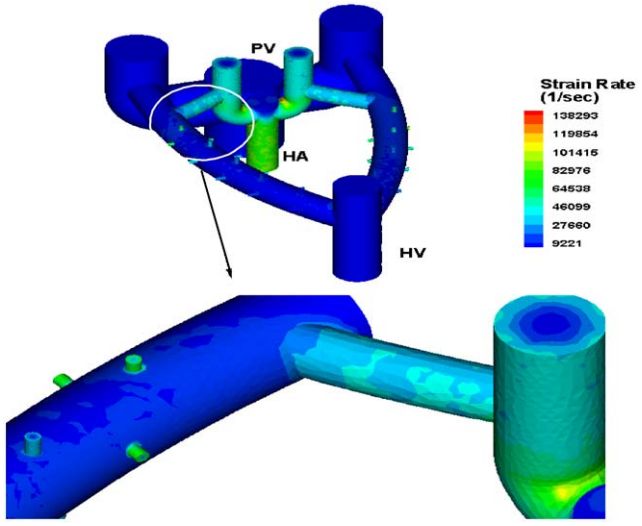

Fig. 15. The simulated strain rate on the PV, HA, sinusoidal space, fenestrations and HV vessel walls.

The strain rate on the vessel walls is plotted in Fig. 15. It is observed that the HA and area I fenestrations have higher strain rates than those in the PV, HV and areas II and III fenestrations. From the previous observations, it is observed that the pressure and velocity are higher in the HA and also in area I compared to those in the PV and areas II and III. Hence, these high velocites in the HA and area I are responsible for the high strain rates in these areas. Since areas II and III fenestrations are located away from the simulated high-pressure portal tract, they are subjected to have lower strain rates than that in area I fenestrations.

5. Conclusions

The present study deals with some basic flow structures in the proposed liver lobular model that incorporates two inlet flows from the arteriole and venule with different fluid properties. The outlet of the lobular structure consisted of a fenestrated sinusoidal path and an open ended HV. The sinusoidal space was split as pre, inter and post-sinusoidal space. These spaces are mentioned as areas I, II and III and are part of zones I, II and III, respectively, in the acinar model. Based on the simulated results of the microscale lobular model, the available findings from the present study and the previous reports were unified. The finite volume approach was employed to solve this non-Newtonian microvessel blood flow.

The Power law model and the Walburn and Schenck model were used to calculate the blood viscosity. The Power law model was found to turn to a Newtonian model at higher strain rates. But in the Walburn and Shneck model, the viscosity kept decreasing with strain rate. The axial velocity profile for the Newtonian fluid was parabolic whereas for the non-Newtonian fluid it was flattened. The flattening velocity profile was due to the shear thinning property of the blood. For validation purposes, the numerical results were compared with the results of Chung et al. (2003) for a 180° bend. A good agreement was found.

In the vessels, velocity and pressure contours and profiles were plotted along the axial cross sections at various time intervals. It was observed that at the sinusoidal entrance, the pressure and velocity showed much higher values with respect to time and location. This trend was attributed to the proximity of the portal tract region. The velocity and pressure decreased as the distance between portal tract and sinusoidal space increased. It was found that the HA pressure was essential to drive the flow. Since the pressure of the HA

was much higher than the PV, the arteriole blood swept the blood from the venule, without mixing the PV blood and HA blood. When the pressure drop occurred in the arteriole, the flow was sustained owing to the pressure difference in the venules. Lautt (1980) reported a similar observation. He showed that the intermittency due to the arteriolar sphincter could enable hepatic flow without mixing the arteriole and portal blood. Also separation lines in the entry flow were found due to the bifurcations present at the arteriole and venule. Similar detachment lines were also observed in the open-ended HV blood flow.

The pressure contours in area III fenestration at two different times were plotted and analysed. These contours revealed that a sufficiently high HA pressure is required to have a unidirectional flow in the acinus. This result coincides with the report of Katz and Rodbard (1939). They have also reported that the portal blood flow in zone III or in the post-sinusoidal is not unidirectional all the time.

Eddies were observed at the intersection plane of fenestrations and sinusoidal space. The size of the eddies was found to decrease while the zonal level increased. The mass flow rate was calculated in three areas. The results showed that area I cells receive more blood compared to those in areas II and III. MacPhee et al. (1993) and Bouwens et al. (1986) found that in zone I the Kupffer cells occurs greater in numbers compared to zones II and III. These observations correspond to the present results as a greater drainage of blood occurred in area I compared to areas II and III and hence more cleaning activity is required in area I.

The secondary flow patterns were observed near the intersection planes of fenestrations and sinusoidal path. The Dean vortices were found to decrease with the increase of the sinusoidal length. The high pressure in the HA and in area I led to high strain rates at these vessel walls.

The knowledge regarding the three-dimensional non-Newtonian blood flow characteristics in a hepatic lobular model has been gained by using computational fluid dynamic technique. These currently simulated results will set important guidelines for understanding the impact of pressure variations in the acinus and their consequences on the diagnosis of liver diseases.

Acknowledgement

This research is financially supported by the National Science Council of R.O.C under the NSC 92-2218-E-002-026-YF. The authors would like to express their thanks to Dr. Marc Thiriet and P.H. Lee for their kind support and encouragement in the course of this study.

References

Andrews, W.H., 1979. Liver. Edward Arnold (Publishers) Limited, New York.

Arias, I.M., Jakoby, W.B., Popper, H., Schachter, D.A., Shafritz, D.S., 1988. The Liver Biology and Pathobiology. Raven Press, New York.

Bezy-Wendling, J., Krętowski, M., Rolland, Y., 2003. Hepatic tumor enhancement in computed tomography: combined models of liver perfusion and dynamic imaging. Computers in Biology and Medicine 33, 77–89.

Bitsch, L., 2002. Blood flow in microchannels. Master Thesis, Technical University of Denmark, Denmark.

Bouwens, L., Baekland, M., De Zanger, R., Wisse, E., 1986. Quantitation, tissue distribution and proliferation kinetics of Kupffer cells in normal rat liver. Hepatology 6, 708–712.

Bovendeerd, P.H.M., van Steenhoven, A.A., van de Vosse, F.N., Vossers, G., 1987. Steady entry flow in a curved pipe. Journal of Fluid Mechanics 177, 233–246.

Branemark, P.I., Lindstrom, J., 1963. Shape of circulating blood corpuscles. Biorheology 1, 139–142.

CFD Research Corporation, 216 Wynn Drive Huntsville, AL 35805, USA.

Chang, W., Trebotich, T., Lee, L.P., Liepmann. D., 2000. Blood flow in simple microchannels. First Annual International IEEE-EMBS Special Topic Conference on Microtechnologies in Medicine and Biology, Lyon, France.

Chen, J., Lu, X-Y., Numerical investigation of the non-Newtonian blood flow in a bifurcation model with a non-planar branch. Journal of Biomechanics, in press.

Chien, S., Usami, S., Dellenback, R.J., Gregersen, M.I., 1970. Shear dependent deformation of erythrocytes in rheology of human blood. American Journal of Physiology 219, 136–142.

Chung, Y.M., Tucker, P.G., Roychowdhury, D.G., 2003. Unsteady laminar flow and convective heat transfer in a sharp 180° bend. International Journal of Heat and Fluid Flow 24, 67–76.

Daemen, T., Huitema, S., Koudstaal, J., Scherphof, G.L., Hardonk, M.J., 1989. Population kinetics of rat liver macrophages after intravenous administration of liposome-encapsulated MDP. In: Wisse, E., Knook, D.l., Decker, K. (Eds.), Cells of the Hepatic Sinusiod, Vol. 2. Kupffer Cell Foundation, pp. 205–400.

Das, B., Johnson, P.C., Popel, A.S., 1998. Effect of nonaxisymmetric hematocrit distribution on non-Newtonian blood flow in small tubes. Biorheology 35, 69–87.

Fahraeus, R., Lindqvist, T., 1931. The viscosity of the blood in narrow capillary tubes. American Journal of Physiology 96, 562–568.

Fung, Y.C., 1993. Biomechanics: Mechanical properties of Living Tissues. Springer, New York.

Fung, Y.C., 1996. Biomechanics: Circulation, second ed. Springer, New York.

Fung, Y.C., Perrone, N., Anliker, M., 1972. Biomechanics: Its Foundations and Objectives. Prentice-Hall, Englewood Cliffs, NJ.

Gijsen, F.J., van de Vosse, F.N., Janssen, J.D., 1999. The influence of the non-Newtonian Properties of blood on the flow in large arteries: steady flow in a carotid bifurcation model. Journal of Biomechanics 32, 601–608.

Gleen, E., 1998–2004. Thy Physics Hypertextbook.

Hron, J., Malek, J., Turek, S., 2000. A numerical investigation of flows of shear-thinning fluids with applications to blood rheology. International Journal of Numerical Methods and Fluids 32, 863–879.

Katz, L.N., Rodbard, S., 1939. The integration of the vasomotor responses in the liver with those in other systemic vessels. H. Pharmacology and Experimental Therapy 67, 407–414.

Lautt, W., 1980. Hepatic Circulation in Health and Disease. Raven Press, New York.

Lebouton, A.V., 2000. Molecular and Cell Biology of the Liver. CRC Press, New York.

Ledezma, G.A., Folch, A., Bhatia, S.N., Balis, U.J., Yarmush, M.L., Toner, M., 1999. Numerical model of fluid flow and oxygen transport in a radial-flow microchannel containing hepatocytes. Journal of Biomechanical Engineering 121, 58–64.

MacPhee, P.J., Schmidt, E.E., Groom, A.C., 1993. Organization and flow in the liver Microcirculation. In: Messmer, K., Menger, M.D. (Eds.), Liver Microcirculation and Hepatobirliary Function. Progress in Applied Microcirculation vol. 19. pp. 52–73.

McCuskey, R.S., 1994. The hepatic microvascular system. In: Arias, I.M., Boyer, J.L., Fausto, N., Jakoby, W.B., Schachter, D.A., Shafritz, D.A. (Eds.), The Liver Biology and Pathobiology. Raven Press, New York, pp. 10–20.

Michalopoulos, G.K., DeFrances, M.C., 1997. Liver regeneration. Science 276, 60–65.

Mountcastle, V.B., 1968. , 12th ed. Medical Physiology, vol. 1. The C.V. Mosby Company, St. Louis.

Paton, R.C., Nwana, H.S., Shave, M.J.R., Bench-Capon, T.J.M., 1992. Computing at the tissue/organ Level. Proceedings of the First European Conference on Artificial Life, MIT Press, Paris.

Ruijter, J.M., Markman, M.M., Hagoort, J., Moorman, A.F., Lamers, W.H., 2000. Relative distance: the key to the shape of hepatic building blocks. Image Analysis and Stereology 19, 19–24.

Scherphof, G.L., Koning, G., Bartsch, M., Kamps, Y.X., 2002. Targeting liposomes and lipoplexes to cells in the liver. Journal of Cellular and Molecular Biology Letters 72, 251–254.

Seeff, L.B., 2002. Natural history of chronic hepatitis C. Hepatology 36, s35–s46.

Selle, D., Preim, B., Schenk, A., Peitgen, H.O., 2002. Analysis of vasculature for liver surgical planning. IEEE Transactions on Medical Imaging 21, 1344–1357.

Sllen, J.W., Bhatia, S.N., 2002. Engineering liver therapies for the future. Tissue Engineering 8, 725–737.

Svihus, B., Edvardsen, D.H., Bedford, M.R., Gullord, M., 2000. Effect of methods of analysis and heat treatment on viscosity of wheat, barley and oats. Animal Feed Science and Technology 88, 1–12.

Thurston, G.B., 1973. Frequency and shear rate dependence of viscoelasticity of human blood. Biorheology 10, 375–381.

Thurston, G.B., 1979. Rheological parameters for the viscosity, viscoelasticity and thixotropy of blood. Biorheology 16, 149–162.

Villeneuve, J., Dagenais, M., Huet, P., Roy, A., Lapointe, R., Marleau, D., 1996. The hepatic microcirculation in the isolated perfused human liver. Hepatology 23, 24–31.

Walburn, F.J., Schneck, D.J., 1973. A constitutive equation for whole human blood. Biorheology 13, 201–210.

Watanabe, Y., Puschel, G.P., Gardemann, A., Jungermann, K., 1994. Presinusoidal and proximal intrasinusoidal confluence of hepatic artery and portal vein in rat liver: functional evidence by orthograde and retrograde biovascular perfusion. Hepatology 19, 1198–1207.